Available online at www.sciencedirect.com
ScienceDirect
Intermetallics 16 (2008) 10–15
Intermetallics
www.elsevier.com/locate/intermet

In situ synchrotron SAXS study of nanocrystallization in $Zr_{65}Ni_{25}Ti_{10}$ metallic glass

X.J. Liu [a], X.D. Hui [a], G.L. Chen [a,*], M.H. Sun [b]

[a] *State Key Laboratory for Advanced Metals and Materials, University of Science and Technology Beijing, Beijing 100083, PR China*
[b] *Department of Physics, Harbin Normal University, Harbin 150025, PR China*

Received 26 April 2007; received in revised form 24 June 2007; accepted 29 June 2007
Available online 19 September 2007

Abstract

The nanocrystallization of $Zr_{65}Ni_{25}Ti_{10}$ metallic glass has been investigated by exploiting *in situ* small angle X-ray scattering (SAXS) coupled with wide-angle X-ray diffraction (XRD) and transmission electron microscopy (TEM) techniques. *In situ*, time-resolved SAXS data reveal that composition decomposition regions with a size of 15.3 ± 0.7 nm exist in the as-prepared sample and nanocrystallized products with a scale of 17.4 ± 0.7 nm occur when the sample is annealed at 615 K up to 3 min. The XRD and TEM results show that the crystallized phases are mainly face-centered cubic (fcc) Zr_2Ni intermetallic compound accompanied by a few closely-packed hexagonal (hcp) ω-Zr(Ti) solid solutions and the particle size is consistent with SAXS results.

Keywords: B. Glasses, metallic; B. Phase transformations; F. Diffraction

1. Introduction

Metallic glasses, for their unique structures and excellent properties in contrast to the conventional crystalline materials, have attracted comprehensive attention since the first Au–Si glass was obtained in 1960s [1]. In particular, the appearance of bulk metallic glasses (BMGs) [2–4] has stirred a tide of study, because they could be used as a structural material in engineering applications. However, metallic glasses are thermodynamically metastable and will be devitrified upon annealing, mechanical deformation [5] or high-pressure treatment [6]. Moreover, devitrification can be expected to destroy those novel properties; e.g., devitrification will embrittle the metallic glasses. On the other hand, partial or full crystallization of metallic glasses can create new novel properties or materials, such as nanocrystalline materials can be obtained from the amorphous crystallization method [7]. Therefore, it is of importance to investigate the crystallization of metallic glasses.

Zr–Ni–Ti ternary system has been investigated extensively in the quasicrystalline area, because a stable icosahedral quasicrystalline phase (I phase) can be obtained in the $Ti_{41.5}Zr_{41.5}Ni_{17}$ alloy [8]. However, few attempts have been focused on the amorphous field in this ternary system although it is a common subsystem in many Zr-based BMGs [4,9,10]. Molokanov and Chebotnikov [11] have determined the amorphous and quasicrystals' formation ranges and the glass forming ability (GFA) in the rapidly solidified Zr–Ti–Ni alloys. Yi et al. [12] have studied the structure transformation of $Zr_{47}Ni_{30}Ti_{23}$ amorphous ribbons upon crystallization. In our previous work [13,14], the phase transformation and crystallization kinetics of metallic glass $Zr_{65}Ni_{25}Ti_{10}$ (at.%) alloy have been studied.

In this paper, we further study the correlation of structure as-cast with the nanocrystallized products by adopting *in situ* small angle X-ray scattering (SAXS) coupled with wide X-ray diffraction (XRD) and transmission electron microscopy (TEM) techniques. The data show that there are composition decomposition regions with nanometer scale in the as-cast structure and the size of nanocrystals formed upon annealing

* Corresponding author.
E-mail address: glchen@skl.ustb.edu.cn (G.L. Chen).

0966-9795/$ - see front matter © 2007 Elsevier Ltd. All rights reserved.
doi:10.1016/j.intermet.2007.06.014

has a compatible scale of the decomposition regions. The variation of the size of particles with the annealing time is discussed.

2. Experimental methods

$Zr_{65}Ni_{25}Ti_{10}$ alloy was prepared by arc melting the mixture of pure metals (≥99.9%, wt%) under a Ti-gettered pure argon atmosphere. The alloy ingots were remelted several times to ensure homogeneity. Amorphous ribbons were produced by the vacuum single roller melt-spinning technique (the diameter of copper roller and line velocity are 200 mm and 35 m/s, respectively). X-ray diffraction (Cu Kα Philips APD-10) and transmission electron microscope (TEM, Philips H800, operating at 200 kV) were exploited to check the structural nature of samples as-prepared or after annealing. The non-isothermal DSC experiment to determine the characteristic temperature was performed in Du Pont 2010 differential scanning calorimeter (DSC) at a heating rate of 40 K/min. High vacuum heat treatment experiments were conducted in a vacuum of 4.0×10^{-3} Pa. The thin foil for TEM analysis was prepared electrolytically by twinjet polishing under 240 K in a mixture of 90 vol% methanol and 10 vol% perchloric acid.

In situ small angle X-ray scattering experiment was performed on 15 μm thickness specimen at beamline 4B9A of Beijing Synchrotron Radiation Facility (BSRF). The energy range of the beamline is from 3 to 12 keV with a resolution of 3×10^{-4} and the photon flux is 1.0×10^{10} photons/s. The wavelength of the incident monochromatic X-ray beam λ is 1.54 Å. The further information of the spectrometer can be seen in Ref. [15]. The temperature of the sample was controlled by a thermal heating accessory with a precision of ±1.0 K [16]. The scattered X-ray intensities were collected using an image plate technique, as a function of the modulus of the scattering vector, $q = 4\pi\sin\theta/\lambda$, where 2θ is the scattering angle. The detector of image plate was Mar3450 with a resolution of 150 μm. The SAXS intensity of samples was obtained from the total measured SAXS intensity subtracting the background scattering and all data were normalized.

3. Results and discussion

The full amorphous structure of as-cast $Zr_{65}Ni_{25}Ti_{10}$ ribbons was confirmed by the XRD and TEM observations [13]. The glass transition temperature T_g and onset temperature of crystallization T_X of this amorphous ribbons determined by the DSC measurements (Fig. 1) at 40 K/min are 601 and 631 K, respectively. Fig. 2 shows the time-resolved SAXS intensity data of $Zr_{65}Ni_{25}Ti_{10}$ metallic glass annealed in the supercooled liquid region at 615 K. A clear interference maximum is visible at $q_{max} \approx 0.041$ Å^{-1} (q_{max}, the q values of the interference peaks) on the scattering curve for the as-cast sample and the interference peak shifts to lower $q_{max} \approx 0.036$ Å^{-1} as the annealing time increases up to 3 min, which agrees with the results reported by Wang et al. [17] and Löffler and Johnson [18]. It is also noted that no significant shifts of q_{max} occur in Fig. 2a and occurs only when the annealing

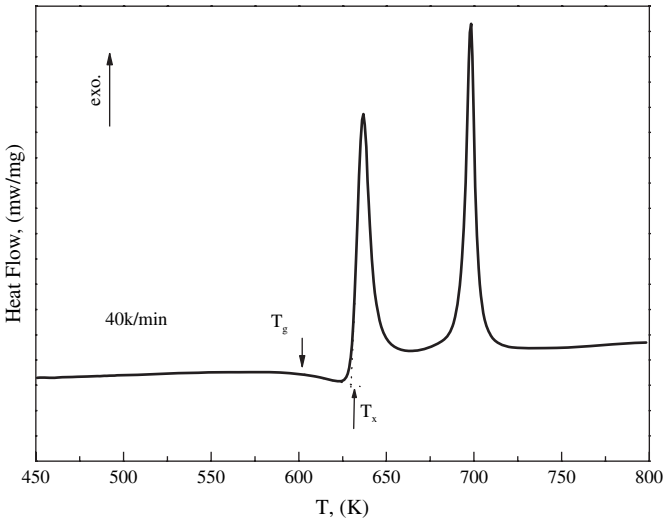

Fig. 1. DSC curve of $Zr_{65}Ni_{25}Ti_{10}$ metallic glass as-cast.

time exceeds 3 min. In particular, after the annealing time up to 15 min, the value of q_{max} retains a constant. The interference maxima give an evidence for composition decomposition or phase separation in the as-cast $Zr_{65}Ni_{25}Ti_{10}$ metallic glass and decomposition or nanocrystallization in the annealed metallic glasses [19]. On the other side, the shift of q_{max} demonstrates that the average size of the composition inhomogeneities varies from the as-cast state to annealed state, due to the fact that the characteristic length L of the materials can be determined by $L = 2\pi/q_{max}$ approximately [19]. The calculation shows that the characteristic length L for as-cast sample is about 15.3 nm and 17.4 nm for the nanocrystallized sample.

According to Porod's law [20], at the linear beam of the Kratky camera, for an ideal two-phase system, i.e., where a clear interface exists between them, the small angle intensity at high q has the asymptotic trend to a constant K, i.e.,

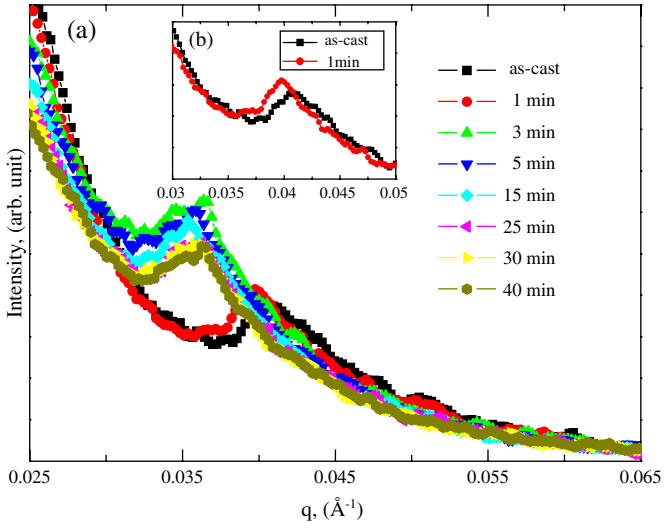

Fig. 2. (a) SAXS intensity data of $Zr_{65}Ni_{25}Ti_{10}$ metallic glass obtained from *in situ* time-resolved SAXS measurements performed at 615 K for different times, as given in the figure; (b) SAXS intensity for short annealing times.

$\lim[q^3I(q)] = K$, where K is Porod constant. In many cases, however, the small angle intensity at high q does not asymptotically attain to a constant K because the systems interested are often not an ideal two-phase system considered. If the interface between two phases is a diffuse transition layer or even not occurred, a negative deviation [21] from Porod's law is expected (Fig. 3b). In contrast, a positive deviation (Fig. 3b) from Porod's law will take place if there are fluctuations in thermal density or some other factors [22,23]. Fig. 3 is the plot of $q^3I(q)$ vs. q^2, i.e., known as Porod plot, where a negative deviation of Porod plot at high q for the as-cast sample and the sample annealed for 1 min can be found while no deviation occurs with increasing annealing time. This gives the evidence that there is no clear boundary among the composition inhomogeneities or decomposition domains in the as-cast sample, before a clear interface appears when annealing time increases to a certain value (3 min for present case). The composition decomposition or phase separation may take place in the $Zr_{65}Ni_{25}Ti_{10}$ metallic liquid and is frozen into glassy state by quenching. Upon annealing for 3 min at 615 K, the crystallization occurs and the clear interface forms between crystallized particles and matrix. Fig. 4 shows the wide-angle XRD patterns of the $Zr_{65}Ni_{25}Ti_{10}$ metallic glass annealed at 615 K for different times. The sample annealed at 615 K for 2 min retains the amorphous structure, however, nanometer scaled face-centered cubic (fcc) Zr_2Ni compounds accompanied by a few closely-packed hexagonal (hcp) ω-Zr(Ti) solid solutions are observed as the annealing time increasing up to 5 min, which are consistent with the SAXS results.

Metastable fcc Zr_2Ni phase is often observed in the primary crystallization of Zr-based metallic glasses [24–26]. Wang et al. [24] found that the fcc Zr_2Ni was the preferentially precipitated phase due to the occurrence of phase separation in the primary crystallization of $Zr_{70}Cu_{20}Ni_{10}$ metallic glass. The fcc Zr_2Ni was also reported by Köster and Meinhardt [25] to form in the crystallization of the amorphous

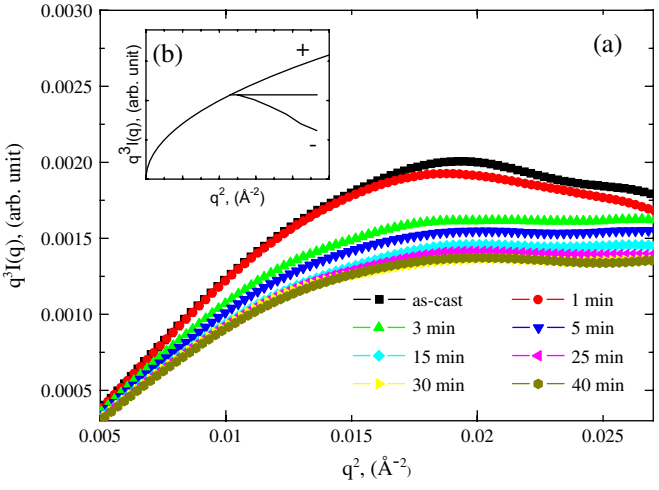

Fig. 3. (a) Porod plots for the SAXS patterns obtained from the sample annealed at 615 K for different times; (b) an illuminating map of the positive (+) and negative (−) deviations from Porod law.

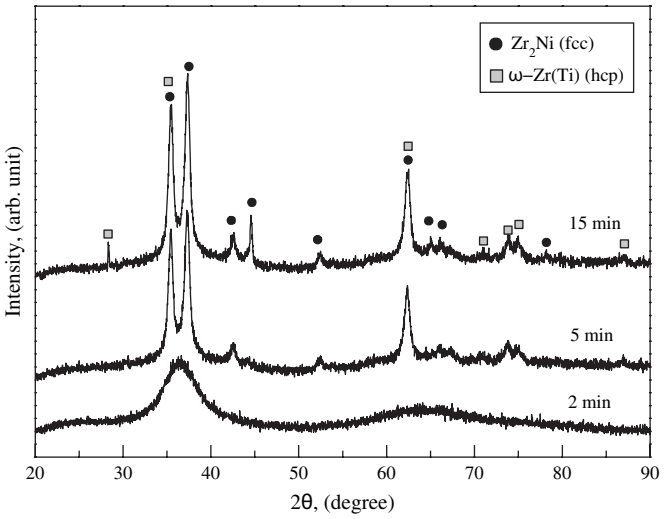

Fig. 4. XRD patterns of $Zr_{65}Ni_{25}Ti_{10}$ metallic glass annealed at 615 K for different times.

$Zr_{60}Al_{15}Ni_{25}$ alloy in the temperature range from 673 to 781 K. These experimental results coincide with our case. On the other hand, some different intermetallic compounds are also frequently reported in the crystallization of Zr-based metallic glasses [27–29]. Li et al. [27] found that the primary phase was not an fcc Zr_2Ni but a hexagonal Zr_6Al_2Ni compound when the $Zr_{60}Al_{15}Ni_{25}$ amorphous ribbons were annealed in the temperature range from 705.5 to 733 K. The different behaviors of primary crystallization are closely related to the chemistry-phase stability and kinetic aspects in the crystallization of amorphous alloys. In our case of $Zr_{65}Ni_{25}Ti_{10}$ alloy, the stable crystallized phase is a bct-Zr_2Ni phase. The Ti alloying does not change the equilibrium phase due to the similar chemical nature between Zr and Ti. Meanwhile, the feature of chemical constituents of the present alloy promotes composition decomposition, which offers a favorable chemical composition condition to form atomic clusters with fcc Zr_2Ni-like structure in the amorphous state. In fact, we have found the existence of fcc Zr_2Ni-like clusters with a scale of 1–2 nm in the as-cast $Zr_{65}Ni_{25}Ti_{10}$ metallic glass by HRTEM coupled with the nano-beam diffraction technique with a spot size of 0.5 nm. Moreover, we also found that these nano-scaled clusters can act as nuclei to directly grow into fcc Zr_2Ni nanocrystals under a large undercooling condition. The related work will be published elsewhere [30]. For the case of $Zr_{60}Al_{15}Ni_{25}$ alloy studied by Li et al. [27] and Köster and Meinhardt [25], one of the stable phases can be hexagonal Zr_6Al_2Ni compound due to strong chemical interaction of Zr with both Ni and Al. However, the kinetic condition of primary crystallization may be favorable to the formation of metastable fcc Zr_2Ni phase. It is well known that the nearest-neighbor atomic arrangement of amorphous alloys has a tendency to be an icosahedron structure [31]. In view of the fact that the atomic configuration of fcc Zr_2Ni structure is very similar to the icosahedron structure [32]. It can help to understand why the primary metastable phase in the case of Köster's work was fcc Zr_2Ni. Here, we note Li's

argument that different levels of oxygen can be another factor to promote the formation of fcc Zr_2Ni metastable phase.

It is important to investigate the relationship between particle size and annealing time in the crystallization process. The time-resolved SAXS experiment is one of the best means for investigating the crystallization kinetics. In the low q region, the SAXS intensity obeys the approximate law of Guinier [33] for intensity $I(q)$, i.e. $I(q) = I(0)\exp(-R_g^2q^2/3)$, where $I(0)$ is the SAXS intensity at $q = 0$ and R_g the electronic radius of gyration of the particles. It is noted that R_g can then be 'defined by the magnitude of the slope of the curve of $\ln I(q)$ vs. q^2 at the origin. Based on the TEM observation (Fig. 5), the precipitated particles can be approximated by spherical particles. Thus, the effective radius R of particles or decomposition domain can be obtained from the correlation $R = \sqrt{5/3}R_g$. Guinier analysis over the q range 0.042–0.050 $Å^{-1}$ yields the size of decomposition zones in as-cast sample and particle size in crystallized sample, which is shown in Fig. 6. The time evolution of particle size (Fig. 6) shows that the Guinier size D_g $(= 2R_g)$ of decomposition zones is of about 12.0 ± 0.5 nm and corresponding effective size D $(= 2R)$ is of around 15.3 ± 0.7 nm before nanocrystallization. Upon the annealing time up to 3 min, the D_g jumps to 13.4 ± 0.5 nm and then increasing the D to 17.4 ± 0.7 nm for nanocrystals, which is consistent with the results estimated from the XRD and TEM observations. Thereafter, the particle size has no significant variation along the increasing annealing time.

Composition decomposition or phase separation is often reported in the Zr-based metallic glasses. Busch et al. [34] have reported that there exist Zr-rich and Be-rich regions in the $Zr_{41.2}Ti_{13.8}Cu_{12.5}Ni_{10.0}Be_{22.5}$ (Vit1) glass by field ion microscopy (FIM) analysis and found that the scale of the phase separation is of the order of 20 nm. Wang et al. [17] have investigated another Zr-based metallic glass $Zr_{52.5}Cu_{17.9}Ni_{14.6}Al_{10.0}Ti_{5.0}$ (Vit105) by *in situ* small and wide-angle scattering measurements using high-energy X-ray at synchrotron radiation, and they also found the decomposition prior to crystallization. On the contrary, Martin et al. [35] and Kündig et al. [36] have also studied Vit1 and Vit105, but did not find any evidence for prior decomposition in the amorphous state. They believed that the composition fluctuation appears in the early stage annealing results from the crystallization reaction. For the present case, the SAXS and XRD data revealed that phase separation takes place in the as-cast $Zr_{65}Ni_{25}Ti_{10}$ metallic glass, and the Guinier analysis shows the scale of the composition fluctuation domains is of about 17.0 nm, which is consistent with the previous reports [17,34]. Supposing the composition fluctuation is due to the partitioning of the constituent elements by the crystallization reaction, in other words, the composition fluctuation is attributed to the

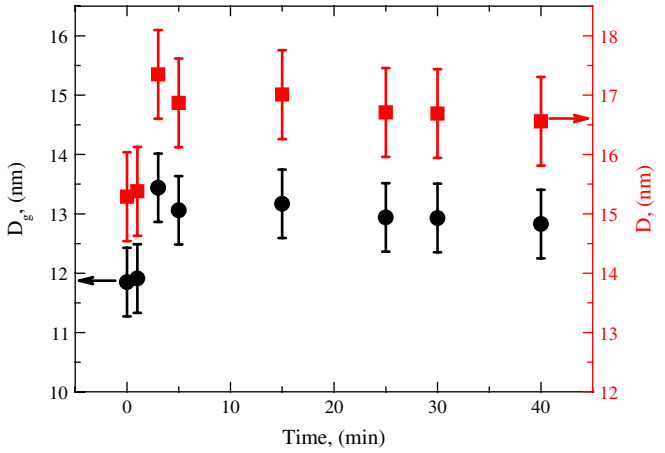

Fig. 6. Evolution of Guinier size D_g and effective size D with annealing time of $Zr_{65}Ni_{25}Ti_{10}$ metallic glass annealed at 615 K.

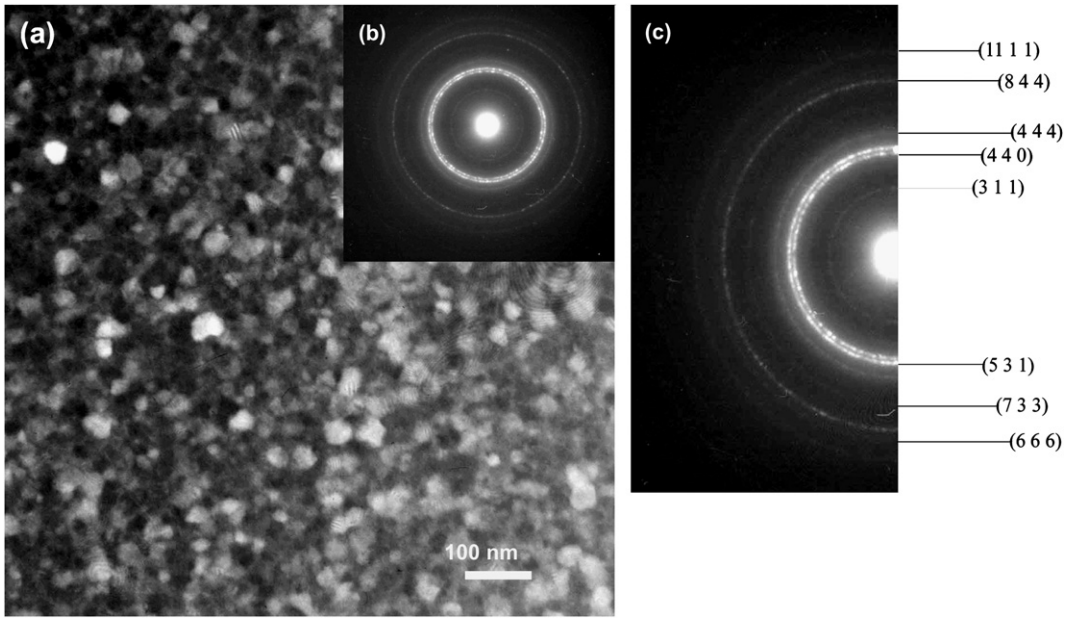

Fig. 5. TEM bright image (a), corresponding SAED pattern (b) and indexed results (c) of $Zr_{65}Ni_{25}Ti_{10}$ metallic glass after annealing at 615 K for 15 min.

formation of the nanocrystals with a scale of about 17.0 nm, then a clear interface between the nanocrystals and the amorphous matrix should appear and the nanocrystals should be reflected in the XRD examination. However, the fact is that neither a clear interface (Fig. 3) nor an appreciable crystalline peak was found even in the sample annealed for 2 min (Fig. 4). Therefore, it is convincing that composition decomposition has occurred in the metallic liquids or the supercooled melts of $Zr_{65}Ni_{25}Ti_{10}$ alloy. From a thermodynamic point of view, liquid phase separation is possible if the free energy–concentration curve of supercooled liquid is convex upward with two minima, because spontaneous decomposition decreases total free energy. For our case, the constituent element Zr has a large negative enthalpy of mixing −49 kJ/mol with Ni but zero with Ti as well as Ti also has a large negative enthalpy of mixing −35 kJ/mol with Ni [37]. This favors the development of the free energy–concentration curve of supercooled liquid with a characteristic of having two minima, corresponding to two distinct clusters; one is comprised of Zr and Ni elements and the other includes Ti and Ni elements. Since the glassy state essentially is the frozen liquid structure, it is not surprised that the phase separation phenomenon was observed in the $Zr_{65}Ni_{25}Ti_{10}$ metallic glass.

The sluggish growth kinetic indicated by the evolution of particle size with annealing time (Fig. 6) attributes to the long-range diffusion and atomic mobility. It is known that the nucleation of crystals needs only short-range diffusion of elements due to the fact that a favored concentration fluctuation is offered by the phase decomposition in the metallic glasses. In the present case, the primary crystalline phase is fcc Zr_2Ni, indicating that Ni atoms are involved in the nucleation just as many studies showed [17,36]. The growth of particles, however, requires long-range diffusion of Ni atoms because the diffusion zones surrounding the particles created by the nucleation are Ni depleted. In addition, the atomic mobility of metallic glass forming melts is far lower than that in a simple metallic liquid, due to its viscosity increasing drastically along with the descending of temperature. For example, the long-range diffusivity in $Pd_{40}Ni_{10}Cu_{30}P_{20}$ metallic glass forming liquid is a value on a 10^{-10} m^2 s^{-1} scale, three orders of magnitude slower than in simple metallic liquids [38]. Thus, it is easy to understand that the size of particles retains nearly constant value 17.0 nm during our experimental time when the sample annealed in the supercooled liquid region.

4. Conclusion

The nanocrystallization of $Zr_{65}Ni_{25}Ti_{10}$ metallic glass has been investigated by using *in situ* time-resolved SAXS accompanied by XRD and TEM. The selected results are summarized as follow:

1. The SAXS data offered the evidence that phase decomposition with a size of around 15.3 ± 0.7 nm occurs in the as-cast sample.
2. Nanocrystallization started to proceed when the sample annealed at 615 K for 3 min. The XRD and TEM results showed that the crystallized phases are mainly fcc Zr_2Ni accompanied by a few hcp ω-Zr(Ti) solid solutions.
3. Guinier analysis showed that the scale of particles is around 17.0 ± 0.7 nm, which is comparable to the size of decomposition region. The slow growth kinetic, indicated by the steady size of particles during the experimental time (40 min) at a given annealing temperature, results from long-range diffusion of Ni atoms and lower atomic mobility.

Acknowledgments

The authors would like to thank Beijing Synchrotron Radiation Facility for assigning the beamtime and technical support from the beamline staffs. This research was supported partly by the National Natural Science Foundation of China (Grant nos. 50431030, 50471097, 50171006).

References

[1] Klement W, Willens RH, Duwez P. Nature 1960;187:869–70.
[2] Kui HW, Greer AL, Turnbull D. Appl Phys Lett 1984;45:615–6.
[3] Inoue A, Zhang T, Masumoto T. Mater Trans JIM 1990;31:177–83.
[4] Peker A, Johnson WL. Appl Phys Lett 1993;63:2342–4.
[5] Kim JJ, Choi Y, Suresh S, Argon AS. Science 2002;295:654–7.
[6] Wang WH, He DW, Zhao DQ, Yao YS, He M. Appl Phys Lett 1999;75:2770–2.
[7] Lu K. Mater Sci Eng 1996;R16:161–221.
[8] Kelton KF, Kim WJ, Stroud RM. Appl Phys Lett 1997;70:3230–2.
[9] Lin XH, Johnson WL. J Appl Phys 1995;78:6514–9.
[10] Xing LQ, Görlor GP, Herlach DM. Mater Sci Eng A 1997; 226–228:429–33.
[11] Molokanov VV, Chebotnikov VN. J Non-Cryst Solids 1990; 117–118:789–92.
[12] Yi S, Kim WT, Kim DH, Oh SH, Park DH. J Mater Sci 2001;36:5101–4.
[13] Liu XJ, Hui XD, Jiao JT, Chen GL. Trans Nonferrous Met Soc China 2004;14:858–63.
[14] Liu XJ, Hui XD, Chen GL. Mater Sci Forum 2005;475–479:3385–8.
[15] Dong B, Sheng W, Yang H, Zhang Z. J Appl Crystallogr 1997;30:877–9.
[16] Sun MH, Wu ZH, Liu GR, Chen X, Chen ZJ. Chin Phys Lett 2005;22:664–6.
[17] Wang XL, Almer J, Liu CT, Wang YD, Zhao JK, Stoica AD, et al. Phys Rev Lett 2003;91:265501–4.
[18] Löffler JF, Johnson WL. Appl Phys Lett 2000;76:3394–6. and references therein.
[19] Löffler JF, Thiyagarajan P, Johnson WL. J Appl Crystallogr 2000; 33:500–3.
[20] Porod G. Kolloid Z Z Polym 1951;124:83–114.
[21] Chai ZG, Meng CF. J Appl Crystallogr 1998;31:7–9.
[22] Rathje J, Ruland W. Colloid Polym Sci 1976;254:358–70.
[23] Li ZH, Sun JH, Zhao JP, Wu D, Sun YH, Liu Y, et al. Acta Phys Sin 2000;49:775–80.
[24] Wang HR, Gao YL, Min GH, Hui XD, Ye YF. Phys Lett 2003; A314:81–7.
[25] Köster U, Meinhardt J. Mater Sci Eng A 1994;178:271–8.
[26] Saida J, Matsushita M, Inoue A. J Non-Cryst Solids 2002; 312–314:617–21.
[27] Li JF, Huang ZH, Zhou YH. Intermetallics 2007;15:1013–9.
[28] Jang JSC, Chang LJ, Hung TH, Huang JC, Liu CT. Intermetallics 2006;14:951–6.

[29] Nagase T, Nakamura M, Umakoshi Y. Intermetallics 2007;15:211–24.
[30] Liu XJ, Chen GL, Hui XD, Hou HY, Yao KF, Liu CT, unpublished data.
[31] Sheng HW, Luo WK, Alamqir FM, Bai JM, Ma E. Nature 2006;439:419–25.
[32] Li C, Inoue A. Phys Rev B 2001;63:172201–4.
[33] Guinier A, Fournet G. Small-angle scattering of X-ray. New York: Wiley; 1955.
[34] Busch R, Schneider S, Peker A, Johnson WL. Appl Phys Lett 1995; 67:1544–6.
[35] Martin I, Ohkubo T, Ohnuma M, Deconihout B, Hono K. Acta Mater 2004;52:4427–35.
[36] Kündig AA, Ohnuma M, Ohkubo T, Hono K. Acta Mater 2005;53:2091–9.
[37] Boer de FR, Boom R, Mattens WCM, Miedema AR, Niessen AK. Cohesion in metals. Amsterdam: Elsevier; 1988.
[38] Meyer A, Busch R, Schober H. Phys Rev Lett 1999;83:5027–9.